Dalton Transactions

PAPER

View Article Online
View Journal | View Issue

Cite this: *Dalton Trans.*, 2014, **43**, 3244

Calcium phosphate nanoparticles: a study of their synthesis, characterization and mode of interaction with salmon testis DNA

Milon Banik and Tarakdas Basu*

Calcium phosphate nanoparticles (CPNPs) are presently emerging as a second generation vector for efficient delivery and stabilization of nucleic acids inside cells, although the detailed mode of interaction between CPNPs and DNA is still obscure. This study discloses some features of the interaction. For this study, we synthesized CPNPs by a modified co-precipitation method and characterized the particles by different techniques such as dynamic light scattering, X-ray diffraction, electron dispersive spectroscopy, Fourier transform infra-red spectroscopy, differential thermal and thermo-gravimetric analysis, and atomic force, scanning and transmission electron microscopy. The characterization studies showed that the nanoparticles were spherical in shape, about 45 nm in size and were composed of the hydroxyapatite form of calcium phosphate; almost 90% of the starting materials were converted to nanoparticles (NPs). The different aspects of the interaction between CPNPs and salmon testis DNA were investigated using techniques such as UV-Vis spectrophotometry, circular dichroism, Fourier transform infra-red spectrometry, thermal denaturation, microviscometry, agarose gel electrophoresis, cyclic voltammetry and atomic force microscopy. The results revealed that CPNPs interacted with DNA with ~1 : 3.3 stoichiometry with a binding constant of the order of 10^4 M^{-1} through groove-interacting mode and a single nanoparticle covered about 6.2 base pairs of the DNA chain. Moreover, the binding interaction was spontaneous, cooperative, exothermic and enthalpy-driven and some electrostatic nature of the binding was also evident; however, the non-polyelectrolyte contribution was dominant. The binding interaction finally caused an increase in the melting temperature of DNA from 70.8 °C to 75 °C and alteration of its secondary structure from the naturally occurring B-form to C-form.

Received 13th September 2013,
Accepted 5th November 2013

DOI: 10.1039/c3dt52522h

www.rsc.org/dalton

Introduction

The well-known transfection process consists of the uptake of extraneous DNA molecules and their subsequent maintenance by mammalian cells. In this process, calcium phosphate is widely used to co-precipitate DNA on the cell surface, after which the adsorbed DNA becomes introduced into the cell cytosol through endocytosis.[1] The affinity of calcium phosphate for the phosphate groups in nucleic acids is believed to be the reason for the good adherence of DNA to calcium phosphate. Although DNA is allowed to be precipitated on the cell surface by calcium phosphate, after entry into the cell, the DNA becomes naked; subsequently when it passes through the cell cytosol towards the cell nucleus, it faces degradation in lysosomes and/or by cytosolic nucleases[2] and so the efficiency of traditional transfection processes is very low. Therefore, for efficient transfection, DNA needs to be protected from such attack. For this, present attempts are going on to use calcium phosphate nanoparticles (CPNPs), instead of calcium phosphate, for transfection because CPNPs can penetrate well the cell membrane and remain bound with the transfecting DNA within the cell, so that the DNA cannot be attacked by lysosomes/nucleases and can be stably maintained in the cell cytosol to be finally translocated into the nucleus. CPNPs, due to their good penetrating power across cell membranes, high biocompatibility (as, calcium phosphate is the main component of bone and teeth) and binding ability with DNA, are, therefore, considered to be a second generation vector for efficient delivery and stable maintenance of genes inside cells.[3–5] There is a report of the preparation of nanoparticles with a calcium phosphate core followed by a DNA layer, further followed by a calcium phosphate shell.[6] Such multi-shell nanoparticles are found to protect DNA from intracellular degradation by nucleases in cultured endothelial cells. Like DNA, RNA can also be introduced into the cell by CPNPs. In a gene silencing/antisense experiment, siRNA-bound CPNPs are

Department of Biochemistry and Biophysics, University of Kalyani, Kalyani – 741235, West Bengal, India. E-mail: tarakdb@yahoo.com; Fax: +91 33 25828282

found to inhibit the green fluorescence from HeLa-EGFP cells.[7]

While much emphasis has been given to CPNP-mediated DNA delivery, no systematic study has reported on CPNP–DNA interactions. Here, we report some aspects of the DNA–CPNP interaction. In order to carry out the study, we synthesized CPNPs in an innovative way. There are different reported methods of preparing CPNPs, such as solid state reaction,[8] chemical precipitation,[9,10] hydrothermal reaction,[11,12] solvothermal method,[11,13] sol–gel synthesis,[9,10] flame spray pyrolysis,[14] microemulsion,[15,16] electrodeposition[17] *etc.* Our method of preparation of CPNPs was a co-precipitation technique with innovative modifications to two earlier reported methods,[18,19] by which the technique became quite simple and fast. The synthesized nanoparticles were characterized and subsequently their interaction with salmon testis (ST) DNA was investigated. The ST-DNA was chosen because there are numerous reports where to investigate the interaction between DNA and any organic or inorganic ligand, either salmon testis or calf thymus (CT) DNA was generally used due to their high availability and low cost.

Experimental

Materials

For the synthesis of CPNPs, the chemical reagents – calcium nitrate, diammonium hydrogen phosphate and sodium citrate – were purchased from Sigma-Aldrich, USA and were used without further purification. To study the CPNP–DNA interaction, salmon testis (ST) DNA (sodium salt) was also purchased from Sigma-Aldrich. A stock solution of DNA (1.0 mg or 3.03 mM) was prepared by dissolving freeze-dried ST-DNA in 50 mM tris buffer (pH 7.5) over a period of 24 h, followed by mild sonication for 2 min on ice. The bacteriophage λ DNA, restriction endonuclease *Eco*RI and DNase I (of bovine pancreas), used in this study, were procured from Bangalore Genei, India. All other required fine-chemicals were of molecular biology grade.

Preparation of CPNPs

CPNPs were prepared by a co-precipitation method, using calcium nitrate and diammonium hydrogen phosphate as the reactants and Na-citrate as the stabilizing agent. These three ingredients were sterilised separately by autoclaving. 25 ml of an aqueous solution of $Ca(NO_3)_2$, $4H_2O$ (19.51 mM) and 25 ml of an aqueous solution of $(NH_4)_2HPO_4$ (11.94 mM, pH: 10), both kept previously at 80 °C for 30 min, were mixed in a beaker while stirring magnetically at 80 °C for 7 min. 50 ml of 10 mM sodium citrate was then slowly added over 5 min under stirring. The suspension was subsequently sonicated (at 70% amplitude, 20 KHz) in a probe sonicator (Cole-Parmer, CPX 130) for 10 min (in the discontinuous mode: pulse on for 4 s and pulse off for 2 s), when Na-citrate-stabilized CPNPs were produced. The prepared CPNPs were then purified by centrifugation at 40 000 rpm for 20 min at 20 °C in an ultracentrifuge (Sorval, WX Ultra 90) and the NP pellet was washed with and finally re-suspended in Milli-Q water and the supernatant was removed to exclude the unreacted reagents' counter-ions. All the experiments, unless otherwise stated, were performed with these centrifuged and purified NPs.

Characterization of the prepared CPNP

By dynamic light scattering (DLS). Average hydrodynamic size, zeta potential and average molecular weight of the CPNPs were measured by using a DLS instrument (Malvern; Zetasizer).

By X-ray diffraction (XRD). The XRD pattern of CPNPs was recorded using a diffractometer (Bruker, D8) with Cu Kα radiation (λ = 1 : 5408 Å). To prepare the powder sample for XRD, the CPNP solution was first lyophilized in a lyophilizer (Heto, DW-3) and then crushed with a pestle and mortar. The powdered sample was scanned from 10° to 70° 2θ with a 4 s counting time. The average size of the particles was determined from Debye–Scherrer formula $D = (0.9\lambda)/(\beta \cos \theta)$, where D is the diameter of the crystallites, λ is the wavelength of CuKα line, β is the full-width at half-maximum (FWHM) in radians and θ, the Bragg angle.[20] The raw data was refined with respect to 2θ correction, peak asymmetry, change in FWHM, unit cell parameters *etc.*, using Quasor and Profitsoftware programs.

By atomic force microscope (AFM). In this study, a glass cover slip (1 cm^2) for holding the sample was first pretreated with piranha solution (1 : 3 ratio of 30% H_2O_2–concentrated H_2SO_4), then washed copiously with Milli-Q water and subsequently dried by keeping it in a 80 °C oven for 2–3 h. About 25 μl of the 10 times diluted freshly prepared NP suspension was taken on the cleaned cover slip, which was then put in a vacuum desiccator overnight so that a thin film was formed over the cover slip. The dried film was scanned by AFM (Veeco, di-Innova) in tapping mode, using the nanoprobe cantilever made of silicon nitride with a spring constant of 49 N m^{-1}.

By scanning electron microscopy with energy dispersive X-ray attachment (SEM-EDX). The size and shape of the nanoparticles were determined from the FESEM (JEOL JSM-6700F) image and the elemental composition of the CPNPs was obtained from the coupled EDX spectra. The prepared CPNP suspension was first diluted up to 5 times in Milli-Q water and then a drop of the diluted sample was loaded on a carbon tape followed by platinum coating in ultra vacuum. After complete drying in the ultra vacuum, measurements were done.

By transmission electron microscopy (TEM). For this study a drop of the 5 times diluted sample was placed on a carbon-coated copper grid (Applied Biosystems, India) and subsequently dried in a vacuum desiccator. The morphology and size of the NPs were analyzed using a transmission electron microscope (JEOL, JEM-2010).

By Fourier transform infra-red spectroscopy (FTIR). Colloidal CPNP solution was lyophilized to powder form and the KBr pellet, for the FTIR sample, was prepared by mixing 1 mg powdered CPNPs with 250 mg KBr. The spectroscopy was performed on a FTIR machine (Perkin Elmer L 120-000A) in transmission mode, 400–4000 cm^{-1}, and resolution 4 cm^{-1}. The

spectrum was analyzed with respect to the standard IR series data.

By differential thermal and thermo-gravimetric analysis (DTA-TGA). The DT-TG analysis of a material is generally performed to investigate its thermal stability *i.e.*, breakdown to other materials as well as loss of weight with a gradual rise in temperature. This study was performed on the lyophilized CPNP powder, using a DT-TGA analyzer (DTG-60H, Shimadzu) in a nitrogen atmosphere in the temperature range from ambient to 1100 °C, with an increment of temperature at a rate of 10 °C min^{-1}.

By measuring the percentage conversion of the ingredients into CPNPs through (a) a colorimetric inorganic phosphate assay and (b) an EDTA gravimetric titration procedure for calcium. To determine the percentage of the precursors converted to CPNPs, the unused free phosphate and calcium in the CPNP suspension was measured by the colorimetric method of an inorganic phosphate assay with malachite green[21] and a traditional EDTA gravimetric titration procedure for calcium,[22] respectively. The prepared CPNP suspension was centrifuged at 40 000 rpm for 20 min and the supernatant was collected; the free phosphate and calcium concentration in the supernatant was then assayed and finally quantified.

Studies of the DNA–CPNP interaction

By UV spectrophotometric study. In this study, the alteration of the UV spectrum of DNA with stepwise addition of CPNPs was investigated. The study was carried out at 303 K using a Shimadzu (UV160-A) spectrophotometer with a 1 cm path length rectangular quartz cuvette. Since the CPNP suspension had no considerable absorbance in the wavelength region of 230–800 nm, this was added in both the sample and reference cuvettes so that the contribution due to the scattering of CPNP in the DNA spectra was automatically eliminated. The strength and nature of CPNP binding to DNA was found out from the analysis of absorbance data, using the well known Hill equation.[23,24]

For any macromolecule–ligand interaction, the Hill equation is represented as: $\log[\theta/(1-\theta)] = \gamma \log K_b + \gamma \log C_f$, where K_b is the binding constant, γ is the Hill coefficient, C_f is the concentration of free ligand, and θ is the fraction of macromolecule bound to ligand, which is expressed as $\theta = (A_o - A_i)/(A_o - A_r)$, where A_o is the $(\text{absorbance})_{260\ nm}$ of DNA in the absence of CPNP, A_i is the $(\text{absorbance})_{260\ nm}$ of DNA at any CPNP concentration and A_r is the $(\text{absorbance})_{260\ nm}$ of DNA in the presence of the maximum concentration of CPNPs. The plot of $\log[\theta/(1-\theta)]$ *versus* $\log C_f$ represents the Hill plot. The values of K_b and γ are determined from the intercept on *x*-axis (where $\log C_f = -\log K_b$) and the slope in region of the intercept, respectively, of the Hill plot. The importance of γ is that it characterizes the nature of interaction because the values of $\gamma < 1$, $=1$, and >1 signify negative cooperative, non cooperative and positive cooperative binding, respectively.

The stoichiometry for the binding of CPNPs with DNA was measured by the method of continuous variation binding analysis or Job plot analysis.[25,26] Here, the molarities of both the CPNPs and DNA were varied, keeping their total molarity fixed at 150 μM. For a particular molar ratio of DNA : CPNPs, the change of the absorbance ($\Delta_{abs.}$) of the mixture was measured at 260 nm as:

$$(\Delta_{abs.})_{260\ nm} = [(DNA)_{abs.}]_{260\ nm} - [(DNA + CPNPs)_{abs.}]_{260\ nm}$$

The values of $(\Delta_{abs.})_{260\ nm}$ were finally plotted against the molar ratios of DNA and CPNPs (Job plot); the molar ratio, for which the value of $(\Delta_{abs.})_{260\ nm}$ was the maximum, referred to the equilibrium stoichiometric ratio of the DNA–CPNP interaction.

By CD spectrometric study. To understand whether any alteration of DNA conformation occurred due to the binding of CPNPs, a CD spectrometric study was carried out at 25 °C on a Jasco (J-720) spectropolarimeter using a 0.1 cm path length cylindrical quartz cuvette. The CD spectrum of free ST-DNA was first drawn in the wavelength region of 200–320 nm. CPNPs were then added stepwise to the DNA and the spectrum was drawn after each addition. It was checked that CPNPs themselves had no CD in the said wavelength region.

By viscometric study. In order to understand in which mode CPNP interacted with ST-DNA – intercalation or groove-binding – a viscometric study was performed as the most critical test. Viscosity measurements were performed with a micro viscometer (Model Brookfield DVII+pro-v6.3) attached to a water-bath at (30 ± 0.1) °C. The viscosity of DNA alone was first measured, followed by the measurements after addition of increasing concentration of CPNPs into the DNA. After each addition of CPNPs, 1.5 min was allowed to attain thermal equilibrium and then the viscosity was measured. The rotational time of the viscometer stirrer was maintained at 100 rpm and each measurement was repeated five times in order to consider the average of the readings. The data were plotted as $(\eta/\eta_0)^{1/3}$ *versus* *r*, where η and η_0 represented the viscosity of DNA in the presence and absence of CPNP respectively and *r* represented the molar ratio of CPNPs : DNA.

By thermal denaturation or DNA melting study. The heat denaturation of DNA from double-stranded helix to single-stranded coil by gradual rise of temperature, also called DNA melting, was monitored by observing the increase in the absorbance of DNA at 260 nm. The melting profile of ST-DNA *i.e.*, the $(\text{absorbance})_{260\ nm}$ *versus* temperature curve was normally sigmoidal in nature, and the temperature at which the rise in the $(\text{absorbance})_{260\ nm}$ was half of the value of the maximum rise was termed the melting temperature (T_m) of the DNA. In this experiment, DNA with and without CPNPs was heated in the cuvette of the UV-vis spectrophotometer attached to a thermo-regulated circulating water bath and the $(\text{abs.})_{260\ nm}$ was measured to scan the melting profile from 30 °C to 96 °C, keeping the spectrophotometer signal band width at 1.0 nm.

By agarose gel electrophoresis with enzymatic and chemical DNA digestion studies. An agarose gel electrophoresis study was performed to investigate whether the DNA–CPNP complex had retardation of movement compared with the DNA alone, and thus to make the binding of CPNP on DNA more evident.

For this study, 1% agarose gel was used and the electrophoresis was allowed at 5 V cm^{-1} across the electrodes using tris-acetate buffer.[27] The gel, after electrophoresis, was stained with ethidium bromide solution (10 μg) for 35 min followed by de-staining with de-ionized water for 2 h. The gel was finally scanned by the imaging system Typhoon 9210 (GE Healthcare).

Experiments of DNA digestion followed by gel electrophoresis were done to observe whether the CPNP binding on DNA affected the enzyme/chemical-mediated DNA cleavage process. For the DNA digestion study, linear DNA of bacteriophage λ was used instead of linear ST-DNA. For enzymatic digestion, the restriction endonuclease *Eco*RI and the non-specific endonuclease Dnase I were used.[27] Chemical digestion by hydroxyl radicals ($OH^{\bullet}$) was carried out, essentially as described in ref. 28 and 29. A stock solution of iron(II)·EDTA was freshly prepared by mixing 10 μl of 0.2 mM $Fe(NH)_6$ with 10 μl of 0.4 mM EDTA (pH 7.4) and 20 μL freshly prepared 10 mM ascorbic acid. Hydroxyl radicals were generated by allowing this mixture to react with 20 μl of 0.3% H_2O_2. DNA backbone cleavage was initiated by adding 7.5 μL of the final mixture to the λ DNA–CPNP complex. After 1 min, the digestion reaction was stopped by adding 5 μl of 0.1 M thiourea and then the digested DNA was electrophoresed on the 1% agarose gel.

For both gel retardation and DNA digestion studies, linear DNA of bacteriophage λ was used instead of linear ST-DNA. The reason behind choosing λ-DNA was that it was possible to obtain λ-DNA in an intact form, whereas ST-DNA, being large in size compared to λ-DNA, was randomly cleaved into different fragments of different sizes and sequences during extraction. Therefore, during electrophoresis, generally λ-DNA exhibited a single band in the gel, but ST-DNA produced a smear from which the gel retardation result would not be accurately visible. Moreover, since λ-DNA has known specific sites of cleavage by defined restriction enzymes, it produced a definite gel electrophoresis pattern when digested completely with a defined restriction enzyme; obtaining such a definite electrophoresis pattern was not possible for ST-DNA. Thus, to unravel the nature of binding and the different binding parameters between DNA and CPNPs, the randomly fragmented ST-DNA population of low cost could safely be used for all the experiments except the gel electrophoresis, for which λ-DNA was used.

By FTIR study. In order to identify the chemical groups of DNA involved in binding with NPs, FTIR spectroscopy was performed. ST-DNA, dissolved in Tris buffer, was incubated with CPNPs for 30 min at 30 °C and the NP-bound DNA was lyophilized to a powder form. A KBr pellet of the powder was prepared and the FTIR spectroscopy was carried out. This spectrum was analyzed with respect to that of the NP-unbound DNA.

By cyclic voltammetric study. For this study, a cyclic voltammeter BAS-CHI6003D was used, where the reference and working electrodes were Ag/AgCl and Pt, respectively, and the counter electrode was Pt ion. Here 0.2 M tetra-*n*-butylhexafluorophosphate in water was used as a supporting electrode. When the CPNPs and DNA were separately checked, DNA was found to have no voltammogram. Therefore, the interaction was studied here by stepwise addition of DNA to CPNPs. The experiment was performed at 303 K.

By AFM study. To visualize free DNA as well as the DNA–CPNP bound complex separately, 25 μl sample (dissolved in 50 mM HEPES buffer) was taken on mica film, previously incubated with 50 mM $NiSO_4$ solution for 4 h followed by rinsing with Milli-Q water several times. The sample was allowed to fix on the mica surface for 2 h, after which it was washed further with Milli-Q water and finally kept in a vacuum desiccator for over 24 h. The dried film was scanned by AFM, as described above.

Results and discussion

Preparation and characterization of CPNPs

In order to study the interaction between CPNPs and DNA, the CPNPs were prepared in our laboratory. The method of preparation was quite innovative. Two earlier methods[18,19] were modified and amalgamated so that our method of synthesis was very simple and quick. From one method,[18] the precursors (*viz.*, calcium nitrate and diammonium hydrogen phosphate) and some preparatory conditions were adopted, whereas from the other,[19] the stabilizing agent (*viz.*, sodium citrate) was selected. In the first method, a specialized reactor was required, while the second one was very time consuming *i.e.*, it took about 48 hours for the synthesis of the nanoparticles. Our method had no requirement of any reactor; however, inclusion of a sonication step made it possible to synthesize stable, equal-sized nanoparticles within only 50 minutes. Thus our innovation can surely be considered as a new method for preparation of stable colloidal CPNPs, which was also simple and rapid.

The DLS instrument determined the mean hydrodynamic radius of the CPNPs as (160 ± 5) nm with a PDI (poly dispersity index) value of around 0.12 (Fig. 1A), which met the criteria for good quality (homogeneous) sample preparation. Fig. 1B shows that the value of the zeta potential of CPNP was (−) 23 mV at pH 8.0 (which was the final pH of the prepared nanoparticle suspension). The magnitude of zeta potential signifies potential stability of nanoparticles. Large positive or negative zeta potential means particles tend to repel each other, preventing further aggregation/flocculation. Particles with zeta potentials more than ±(30) mV are normally considered stable.[30] From the absolute value of zeta potential of our CPNP, it appeared that the nanoparticles were not stable enough; however, monitoring of size at regular intervals of time by the DLS instrument showed no change in size of the CPNPs within a month of their preparation. Over a month, there was slight increase in particle size indicating a little aggregation or loss of stability of the particles. The DLS instrument also determines the molecular weight (M) of particles in solution from Rayleigh equation – $KC/R_\theta = ([1/M] + 2A_2C)$ – where A_2 is the 2nd virial coefficient (which signifies the

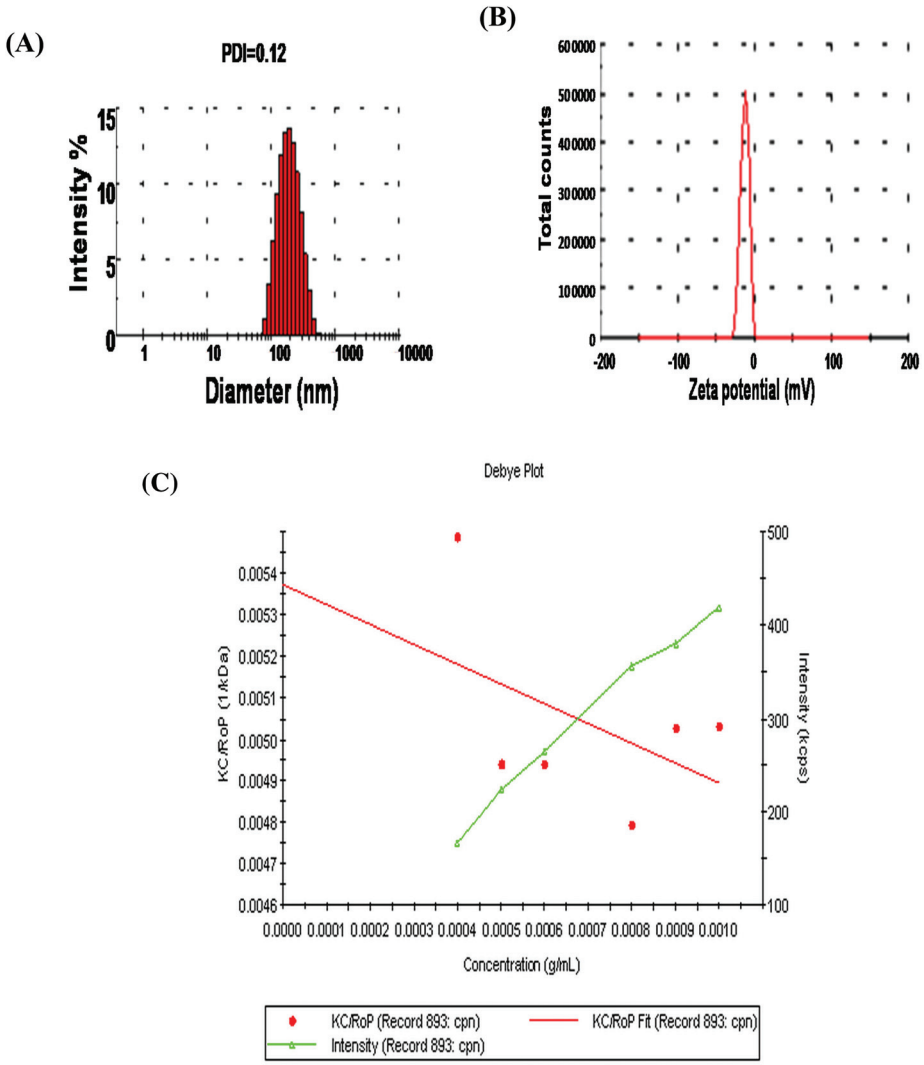

Fig. 1 DLS pattern of (A) size distribution, (B) zeta potential distribution and (C) Debye plot to determine the molecular weight of CPNP.

interaction strength between the particles and the solvent), C is sample concentration, R_θ is ratio of scattered light to incident light and K is a complex optical constant.[31] The instrument plots KC/R_θ *vs.* C, called the Debye plot, of which the intercept on the y-axis determines $1/M$ and the slope determines A_2.[31] For accurate determination of molecular weight, the prepared stock of CPNPs was diluted in different concentrations so that the maximum scattering intensity did not exceed 1000.[31] The green curve of Fig. 1C represents the CPNP concentration *vs.* intensity plot, whereas the red curve represents the derived Debye plot. The result showed that the nanoparticles had an average molecular weight of around (250 ± 30) kDa and the value of the second virial coefficient was −0.00263 ± 0.00163 mol g^{-2}. It should be mentioned here that in the subsequent studies, this DLS-measured molecular weight was used to calculate the molarity of the CPNPs. So far as the significance of the second virial coefficient is concerned, its positive value implies that the particles favor the solvent more than themselves and thus prevents aggregation, a negative value implies that the particles favor themselves more than the solvent and will try to aggregate, and zero value means equivalent interaction between particles and solvent. Here in the case of our CPNPs, the value was very close to zero, which signified its stability in the solvent for days.

Calcium phosphate is known to form more than one crystalline phase. In order of increasing stability, the five distinct phases are dicalcium phosphate anhydrate [$CaHPO_4$] (DCPA), dicalcium phosphate dihydrate [$CaHPO_4{\cdot}2H_2O$] (DCPD), octacalcium phosphate [$Ca_8(PO_4)_4(HPO_4)_2{\cdot}5H_2O$] (OCP), tricalcium phosphate [$Ca_3(PO_4)_2$] (TCP), and hydroxyapatite [$Ca_{10}(PO_4)_6(OH)_2$] (HAP).[32] The hydroxyapatite form of the CPNPs was confirmed from its XRD pattern (Fig. 2), where the peaks at 25.4°, 31.6°, 32.7° and 34° corresponding to the crystal facets (002), (211), (300) and (202), respectively, were the signature peaks of HAP.[33,34] Thus HAP, the most stable form of calcium phosphate, was the constituent component of the

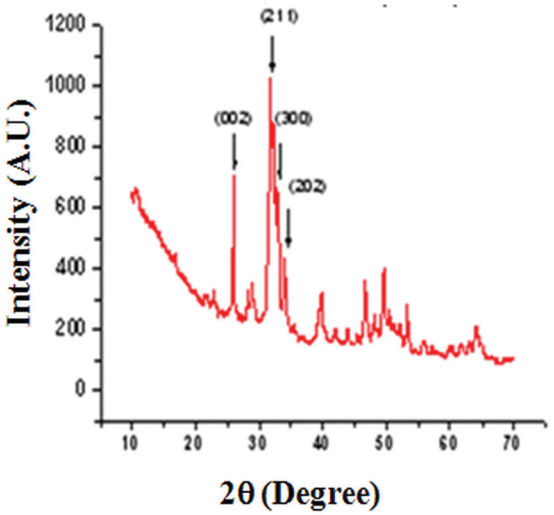

Fig. 2 XRD pattern of CPNPs.

CPNPs. From the Debye–Scherrer formula, the particle size was calculated to be 36.4 nm. This size was nearly three times less than that determined (regularly) by the DLS instrument. In principle, the size determined by DLS, being the hydrodynamic size, always appears somewhat greater than the real size of the core particle as measured by XRD, SEM or TEM.

Fig. 3A shows the AFM image of the nanoparticles; Fig. 3A (I) represents a population of isolated particles in the field of view, Fig. 3A (II and III) represent closer views of a single isolated particle of the said population in 2-D and 3-D mode, respectively, and Fig. 3A (IV) represents the 'line measurement' to denote the size of that particle. The AFM result showed that the CPNPs were round in shape and homogeneous in their size of diameter of about 60 nm. According to the SEM image (Fig. 3B), the nanoparticles were almost round in shape and the diameters of the four randomly selected particles (shown in the image) were 42.4, 45.4, 47.6 and 56.2 nm, implying that the average size of the CPNPs was about 45 nm. Although the SEM result showed that the particle size was slightly smaller than that determined from AFM, both the AFM and SEM studies confirmed the homogeneity in size of the prepared NPs. Therefore, transmission electron microscopy (believed to be the most accurate method of size determination) of the NPs was carried out to get a single isolated particle in the field of view for exact size measurement, which was found to be about 45 nm (Fig. 3C). Moreover, the EDX spectra and the corresponding elemental energy-mass data (Fig. 3D) of the SEM sample clearly demonstrated that the basic elemental composition of CPNP was calcium (mass% = 12.51 ± 2.47), phosphorus (mass% = 7.09 ± 2.06) and oxygen (mass% = 80.40 ± 4.63) and the mass ratio of Ca and P was approximately 1.76 : 1, which was close to Ca : P mass ratio (2.11 : 1) of the precursors calcium nitrate and diammonium hydrogen phosphate used to synthesize the CPNPs.

The production of sodium citrate-stabilized CPNPs was evident from the FTIR spectrum (Fig. 4), where the peaks at 1031.02 cm^{-1}, 601.72 cm^{-1} and 562.65 cm^{-1} represented a phosphate bond and that at 1417.06 cm^{-1} represented an alkaline C–H bond derived from the citrate. Moreover, the peaks at 1628.08 cm^{-1} and 3435.89 cm^{-1} signified C═O and –COOH bonds, respectively, and those at 867.93 cm^{-1} and 771.08 cm^{-1} signified C–H bonds, all associated with citrate stabilization of the NPs.

In order to understand the strength of compactness of the citrate-stabilized hydroxyapatite NPs, DT-TG analysis was done. The TGA curve (as obtained from the instrument), shown in Fig. 5, indicated a weight loss of about 13% (from 6.9 mg to 6.0 mg), when the temperature was gradually raised from 25 °C to 1100 °C. A relatively pronounced mass loss occurred between 25 °C and 600 °C. The DTA curve in Fig. 5 signifies the phase change with rise in temperature. The opposite nature of the peaks at around 175 °C and 390 °C of the DTA curve implied endothermic and exothermic changes, respectively; the peak at 175 °C is attributed to the start of water loss and that at 390 °C signified the start of CO_2 loss.[35] Between 800 °C and 1100 °C, a slight increase in TGA-DTA curves might be due to the decomposition of $Ca_{10}(PO_4)_6$ [HAP] to $Ca_3(PO_4)_2$ and CaO.[36]

In order to find out the percentage of the precursors (calcium nitrate and diammonium hydrogen phosphate) that were converted to the nanoparticles, the unused phosphate and calcium ion concentrations in the synthesized CPNP suspension were measured, as described in the 'Experimental' section. The results of the assays showed that the supernatant of the centrifuged CPNP suspension contained 240 μM inorganic phosphate and 480 μM calcium, which were about 8 and 10% of the precursor diammonium hydrogen phosphate and calcium nitrate concentrations, respectively [concentrations of $(NH_4)_2HPO_4$ and $Ca(NO_3)_2$ originally added were 11.94 and 19.51 mM, respectively, which were diluted 4 times to approximately 3.0 and 5.0 mM in the final CPNP suspension]. This result indicated that about 90% of the precursor substances were incorporated into the CPNPs, or in other words, 90% of the ingredients were converted to NPs.

Interaction between CPNP and ST-DNA

UV-absorption spectrophotomeric study. The $(absorbance)_{260\ nm}$ of ST-DNA dissolved in 50 mM Tris buffer (pH 7.5) decreased gradually with the increasing addition of CPNPs (Fig. 6A), indicating some interaction between DNA and CPNPs. The value of the binding constant (K_b) of the interaction, as determined from the Hill plot (Fig. 6B), was 7.7×10^4 M^{-1} at 303 K and that of the Hill coefficient (γ) was 3.793, implying the nature of DNA–CPNP binding was a positive co-operative interaction. In addition to the temperature 303 K, the experiment was also repeated at two other temperatures *viz.*, 293 K and 313 K. The values of K_b and γ at different temperatures are shown in Table 1. The value of K_b decreased with increasing temperature, which signified gradual weakening of the interaction with the increase in temperature. Using these values of K_b, the values of ΔH (change in enthalpy) and ΔS (change in entropy) of the DNA–CPNP interaction were determined from the van't

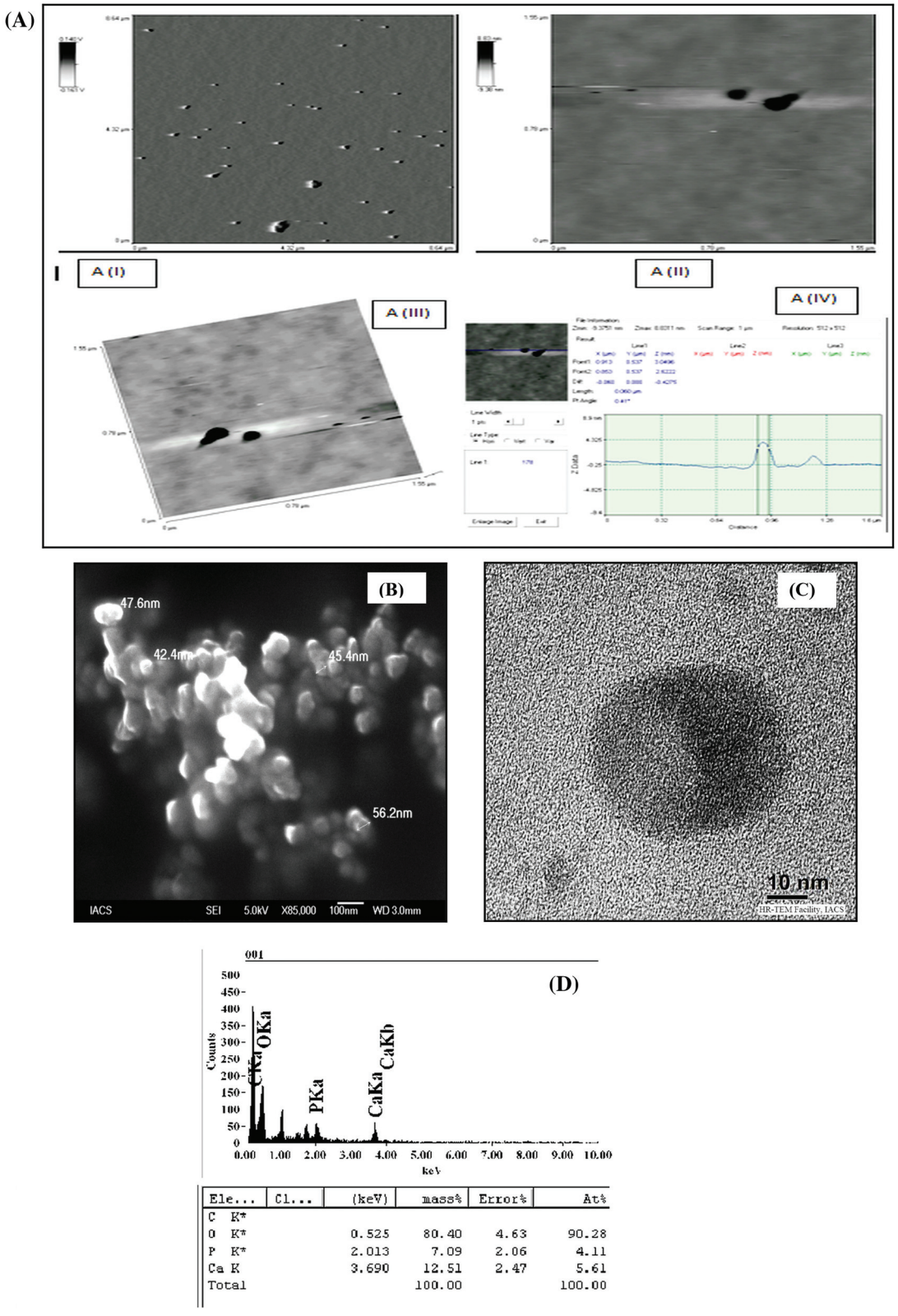

Fig. 3 (A) AFM images, (B) SEM image, (C) TEM image and (D) EDX spectrum with the corresponding elemental energy-mass values of CPNPs.

Hoff equation: $\ln(K_b) = -\Delta H/RT + \Delta S/R$.[37] The van't Hoff plot ($\ln K_b$ *vs.* $1/T$) was found to be linear (Fig. 6C), the slope of which determined ΔH = (−) 1.554 kcal M^{-1} and the intercept on *y*-axis determined ΔS = 0.0172 kcal K^{-1} M^{-1}. The magnitude of the values of ΔH and ΔS signified that the binding reaction was driven by the enthalpy contribution, with a rather

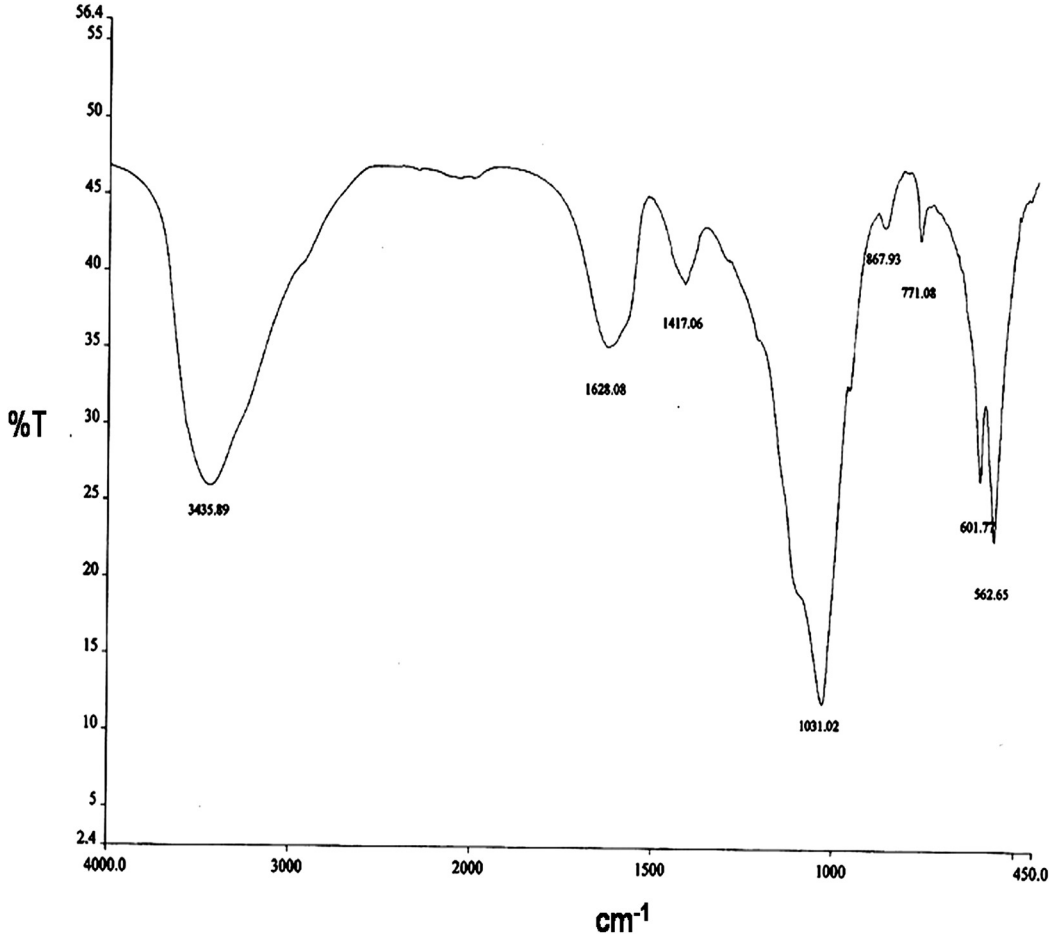

Fig. 4 FTIR spectrum of CPNPs.

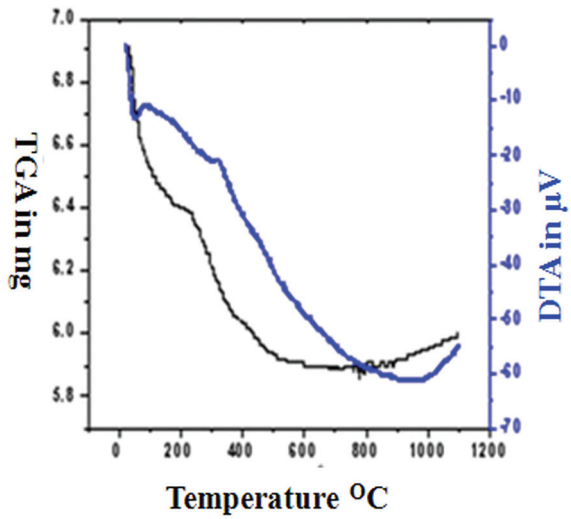

Fig. 5 DTA-TGA curves of CPNPs.

small entropy contribution and the negative value of ΔH implied that the binding interaction was exothermic in nature. Moreover, the values of ΔG (change in free energy) at different temperatures 293, 303 and 313 K, as calculated from the equation $\Delta G = (-)RT \ln K_b$,[38] are shown in Table 1. The negative value of ΔG (at each of the three said temperatures) implied that the DNA–CPNP binding reaction was a spontaneous phenomenon.

To determine the stoichiometric ratio of the DNA–CPNP binding interaction, a Job plot analysis was performed, keeping the total molarity of DNA and CPNPs as 150 μM. From the plot (Fig. 6D), the stoichiometric ratio of DNA : CPNPs was found to be around 3.26 at equilibrium condition.

Salt dependence of the binding phenomenon was studied by observing the fall of DNA absorbance at 260 nm by the gradual addition of CPNPs in the presence of different concentrations of NaCl at 303 K. Fig. 6E shows that the value of the binding constant K_b decreased linearly with the increase of NaCl concentration or in other words, the higher the concentration of Na^+ ions in the medium, the less the binding of CPNPs to DNA. This result clearly indicated that the nature of binding between DNA and CPNPs was electrostatic and the binding affinity of CPNPs on DNA was less than that of Na^+. According to Record's theory of the polyelectrolyte effect, $\delta(\log K_b)/\delta(\log[Na^{+1}]) = -Z\Omega$, where Ω was the fraction of sodium counter ions associated per DNA phosphate and Z was the

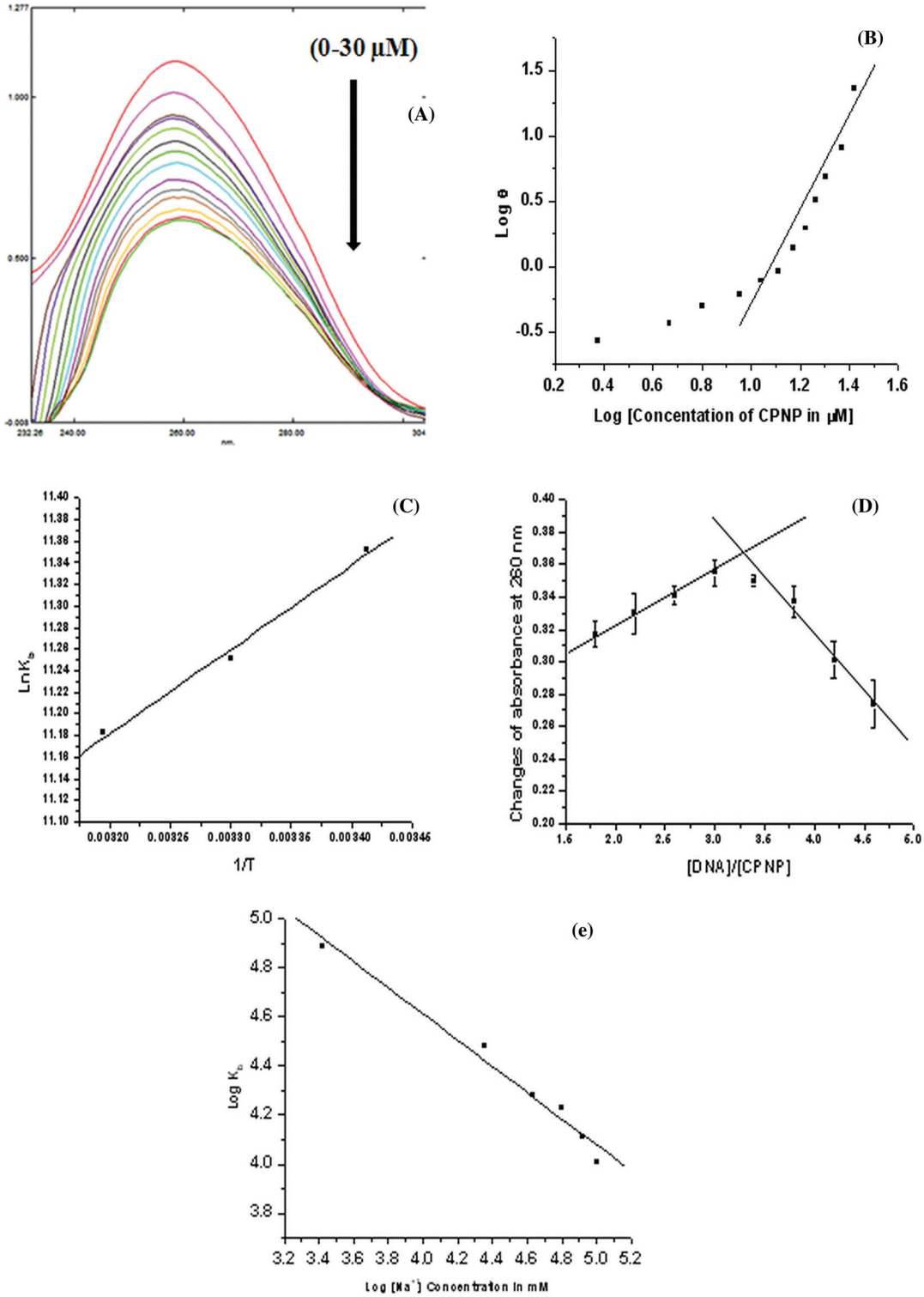

Fig. 6 (A) Changes in UV-absorption spectrum of ST-DNA (162 µM) with stepwise addition of CPNPs (0–30 µM), (B) Hill plot of equilibrium binding between DNA and CPNPs, (C) van't Hoff plot of CPNP–DNA interaction, (D) Job plot with the range of DNA to CPNPs ratio from 1.8 to 4.6, keeping the total molarity of (DNA + CPNPs) as 150 µM, (E) dependence of the binding constant K_b between DNA and CPNPs on the Na^{+1} ion concentration.

apparent charge of the ligand.[39] Therefore, putting the value of $\delta(\log K_b)/\delta(\log[Na^{+1}])$ as the slope of the log K_b *vs.* log[Na^+] plot (Fig. 6E) and the value of Ω as 0.88 for B DNA[25] in the above equation, the apparent charge on CPNP was found to be +0.608. Thus the lesser charge on CPNP (+0.608) than on sodium ion (+1.0) corroborated our result of lesser binding affinity of DNA with CPNPs than with Na^+ ion. From the sodium salt of ST-DNA (where the sodium concentration was

Table 1 Different thermodynamic parameters of CPNP–DNA interaction at three different temperatures

Temp. (K)	$K_b \times 10^3$ M^{-1}	Ln K_b	γ	ΔH (–) kcal M^{-1}	ΔS kcal K^{-1} M^{-1}	ΔG (–) kcal M^{-1}
293	85.18	11.35252	3.460	1.554	0.0172	6.5936
303	76.97	11.25117	3.793			6.7656
313	71.83	11.18206	3.836			6.9376

2.66 mM) used in this study, some Na^+ ions were replaced by CPNPs causing a change in free energy and finally making the DNA–CPNP interaction spontaneous. The polyelectrolyte contribution (ΔG_{pe}) to the total change in free energy (ΔG) of the DNA–CPNP binding was determined from the equation: $\Delta G_{pe} = -Z\Omega \ln[Na^{+1}]$[40] and the non-polyelectrolyte contribution to the binding (ΔG_{npe}) was found out from the equation: $\Delta G = \Delta G_{pe} + \Delta G_{npe}$.[41] Here, the Na^+ ion replacement-derived change in free energy was found to be 28% of the total free energy change of (–) 6.7656 kcal M^{-1} at 303 K (as per Table 1). Therefore, the non-polyelectrolyte contribution (72%) was dominant to the free energy change of the spontaneous DNA–CPNP interaction.

CD spectrometric study. To investigate if there was any alteration of DNA conformation by CPNP binding, a CD spectral study was performed. The CD spectrum of free ST-DNA, dissolved in 50 mM Tris buffer (pH 7.5), had characteristics of B-DNA conformation with a positive peak at ~285 nm due to base stacking and a negative peak at ~240 nm due to helicity (Fig. 7).[42] With the addition of increasing concentration of CPNPs, there was a gradual decrease in the intensities of both the positive and negative bands without any considerable shift of the band peaks. Such CD changes signified some degree of de-stacking of DNA base pairs as well as loss of helicity as a consequence of interaction with CPNPs; no conformational change from the B-form structure (either to A- or Z-form) took place.[42] This type of more relaxed (*i.e.*, de-stacked and untwisted) B-form of DNA has been reported as C-form.[43,44] The CD result can, therefore, be concluded as: the binding of CPNPs to DNA caused local distortions like base un-stacking and untwisting, without any gross alteration in the natural-occurring B-conformation of DNA, but causing a shift from B- to C-form.

Viscometric study. Intercalation or groove-binding are the two most likely binding modes for the agents that bind to DNA non-covalently. These two modes can be distinguished well from the measurement of intrinsic viscosity of DNA, before and after ligand binding. Groove-binding typically results in only subtle changes in structure keeping the DNA essentially in an unperturbed B-form, whereas intercalation results in a substantial change in DNA structure due to insertion of planar ligand moiety between adjacent base pairs, and causes lengthening, stiffening and unwinding of the helix. These changes result in a pronounced alteration of the intrinsic viscosity of DNA in case of intercalation, but not in case of groove-binding.[45–47] Our results revealed that the viscosity of DNA was not at all affected by the increasing addition of CPNPs up to the saturating concentration (Fig. 8), which implied the groove-binding mode of CPNPs on DNA.

DNA melting study. This experiment was done to investigate whether the CPNP binding altered the melting profile of ST-DNA. The denaturation profile of ST-DNA (162 μM ST-DNA 500 μl) dissolved in 50 mM Tris buffer showed that its melting temperature (T_m) was about 70.8 °C, whereas in the presence of CPNP (30 μM), T_m was shifted to 75 °C (Fig. 9). This increase in the value of T_m signified that the binding of the NPs made the DNA double helix more stable. The possible reason behind the increase of T_m was that the CPNP binding lowered the phosphate–phosphate backbone repulsion in DNA. This result strongly corroborated our finding on the groove-binding mode

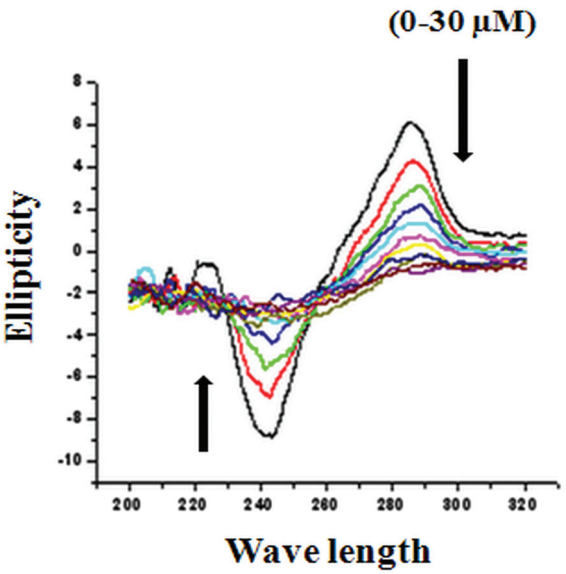

Fig. 7 Changes in the CD spectrum of ST-DNA (162 μM) with stepwise addition of CPNPs up to 30 μM.

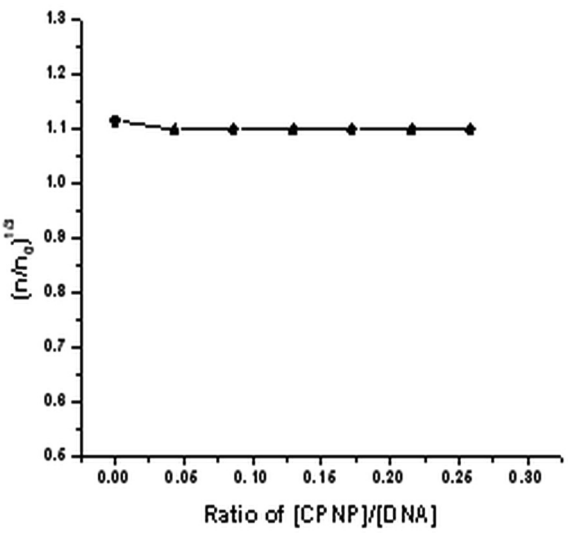

Fig. 8 Intrinsic viscosity of ST-DNA (162 μM) with stepwise addition of CPNPs up to 30 μM.

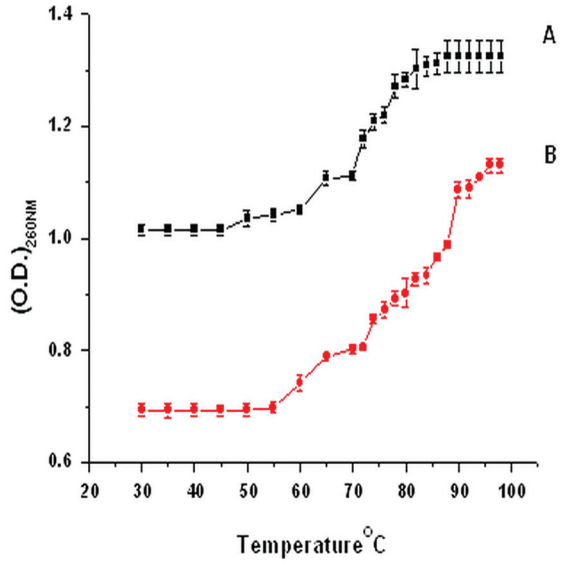

Fig. 9 Alterations in the thermal denaturation profile of ST-DNA (162 μM) with addition of CPNPs (30 μM). A: free DNA and B: DNA–CPNP complex.

of CPNP because in the case of groove binding, the T_m was reported to be increased by 4–5 °C and in case of intercalation, by 7–8 °C.[48] It should be mentioned here that in both cases *i.e.*, in the presence and absence of CPNPs, the value of $(abs.)_{260\ nm}$ of DNA upon complete denaturation was found to increase by about 40% over the value of the non-denatured DNA, and this extent of increase was very close to the standard value.[49] Further, although the concentration of DNA in the absence and presence of CPNPs was the same, the appearance of two different melting profiles was due to lowering of the value of $(abs.)_{260\ nm}$ of DNA on CPNP binding.

The size of the binding site of CPNPs on DNA *i.e.* the number of base pairs over which a CPNP binds, could also be found out from this thermal denaturation study, using the McGhee–von Hipple equation: $(1/T_m^0 - 1/T_m) = (R/\Delta H_{dm})\ln(1 + K_m L)^{1/\sigma}$, where T_m^0 and T_m were the melting temperatures of ST-DNA in the absence and presence of CPNPs, respectively, R was the gas constant, ΔH_{dm} was the enthalpy of DNA melting at T_m^0 (= 8.8 kcal mol^{-1} bp[25]), K_m was the binding constant of DNA–CPNP interaction at T_m, L was the free CPNP concentration and σ was the size of the binding sites.[50,51] Putting the value of K_m, as determined from the extrapolation of the van't Hoff plot (Fig. 6C) at T_m, and the values of T_m^0 and T_m, as determined from this thermal denaturation experiment, in the McGhee–von Hipple equation, the value of 'σ' was calculated to be 6.21. The value of 'σ' as 6.21 signified that in the DNA–CPNP interaction, a single nanoparticle was bound over DNA spanning about 6 base pairs.

Gel retardation and DNA digestion study. This was a direct method to show the formation of any DNA–ligand complex because the complex formation had a retarding effect on the migration of DNA in a gel under electrophoresis. DNA–CPNP complex formation was evident from the smaller migration of the λ-DNA in the presence of CPNPs than in the absence, and the migration rate decreased gradually with the increasing concentration of the NPs (Fig. 10).

Studies of DNA digestion, by both enzymes and hydroxyl radicals, revealed that the CPNP binding did not at all protect DNA from digestion. Fig. 11A shows that the *Eco*RI-mediated

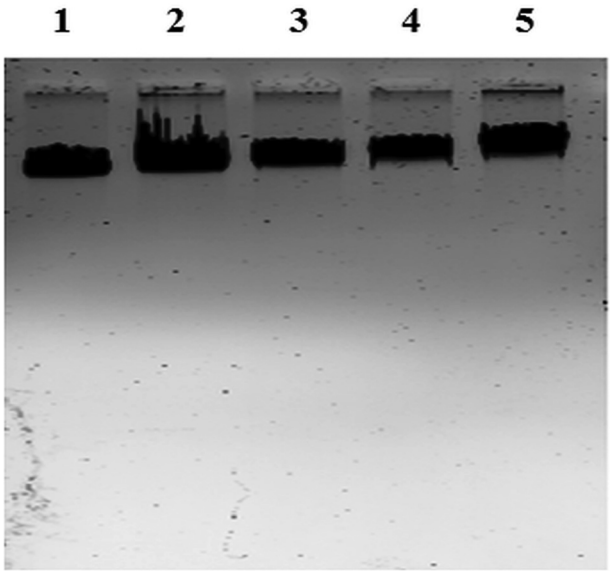

Fig. 10 Gradual retardation of the mobility of λ-DNA (162 μM), bound with increasing concentrations of CPNPs, in 1% agarose gel electrophoresis. The concentrations of CPNPs in lanes 1, 2, 3, 4 and 5 were 0, 15, 20, 25 and 30 μM respectively.

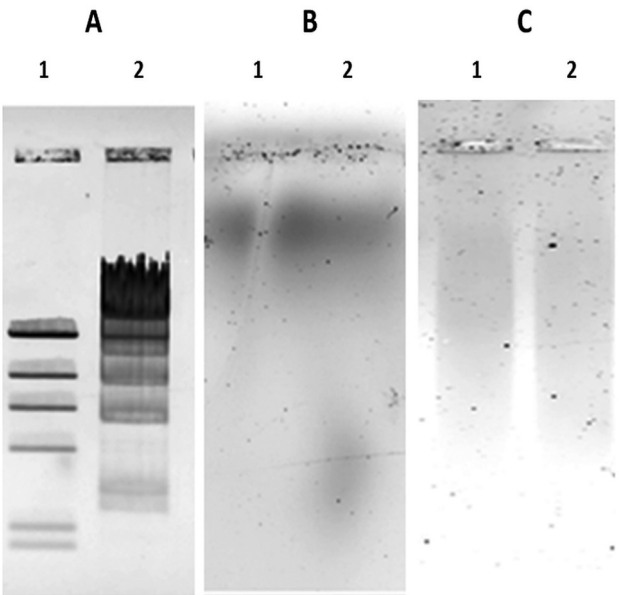

Fig. 11 Enzymatic and chemical digestion patterns of free and CPNP-bound λ-DNA. (A) Digestion by *Eco*RI, (B) digestion by DNase I and (C) digestion by hydroxyl radical. Lanes 1 and 2 represent the digestion patterns of free and CPNP-bound DNA, respectively. In all cases, the concentrations of DNA and CPNP were 162 μM and 30 μM, respectively.

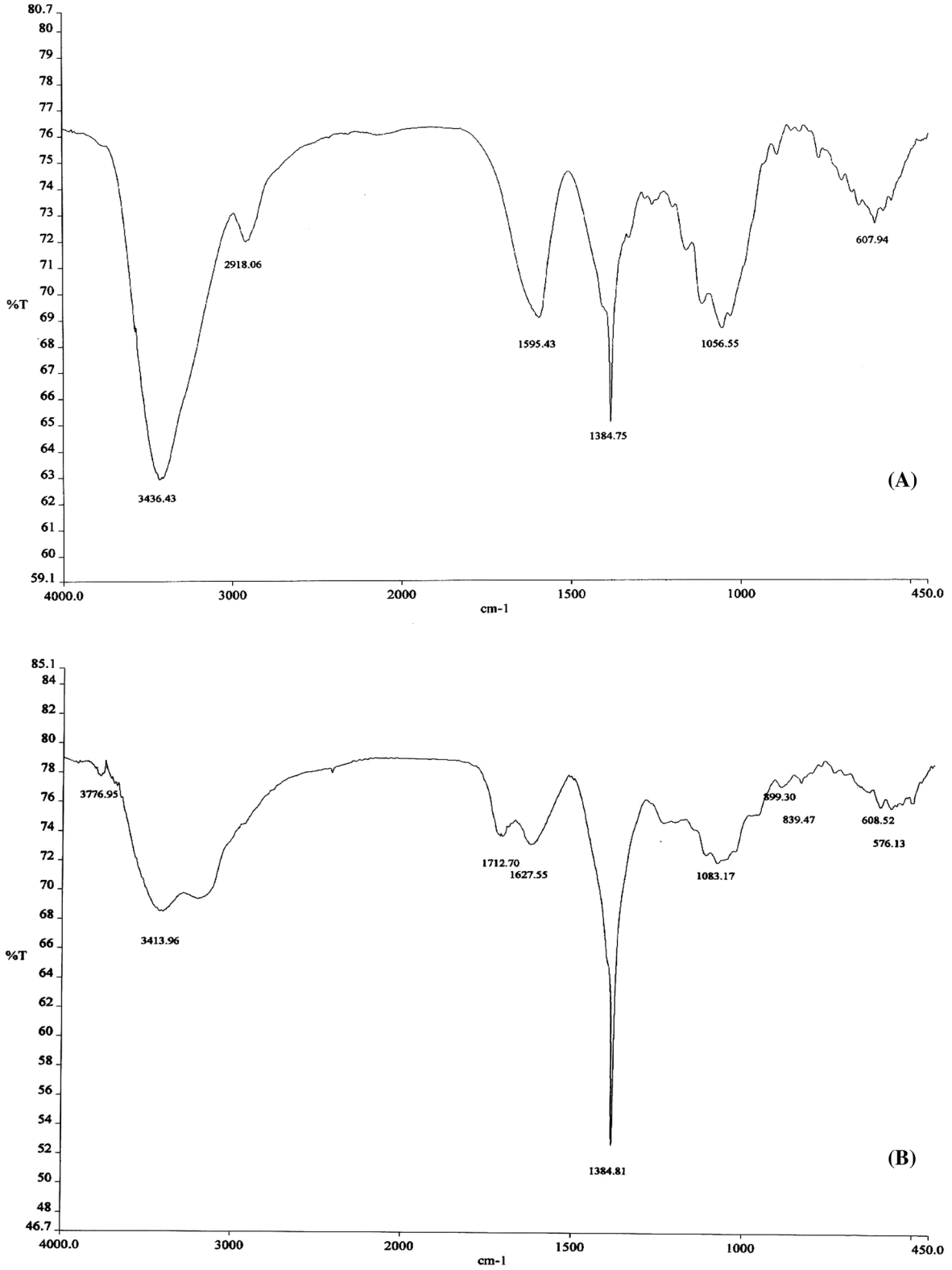

Fig. 12 FTIR spectra of (A) free DNA (162 μM) and (B) CPNPs (30 μM)-bound ST-DNA.

breakage of λ-DNA into six fragments of different sizes was not hindered by the CPNP binding. Fig. 11B and C represent retardation of migration and unhindered cleavage of CPNP-bound λ-DNA by DNase I and $OH^{\bullet}$, respectively. Therefore, our results signified that the CPNP binding of DNA did not affect enzymatic or chemical cleavage on the phosphodiester backbone of

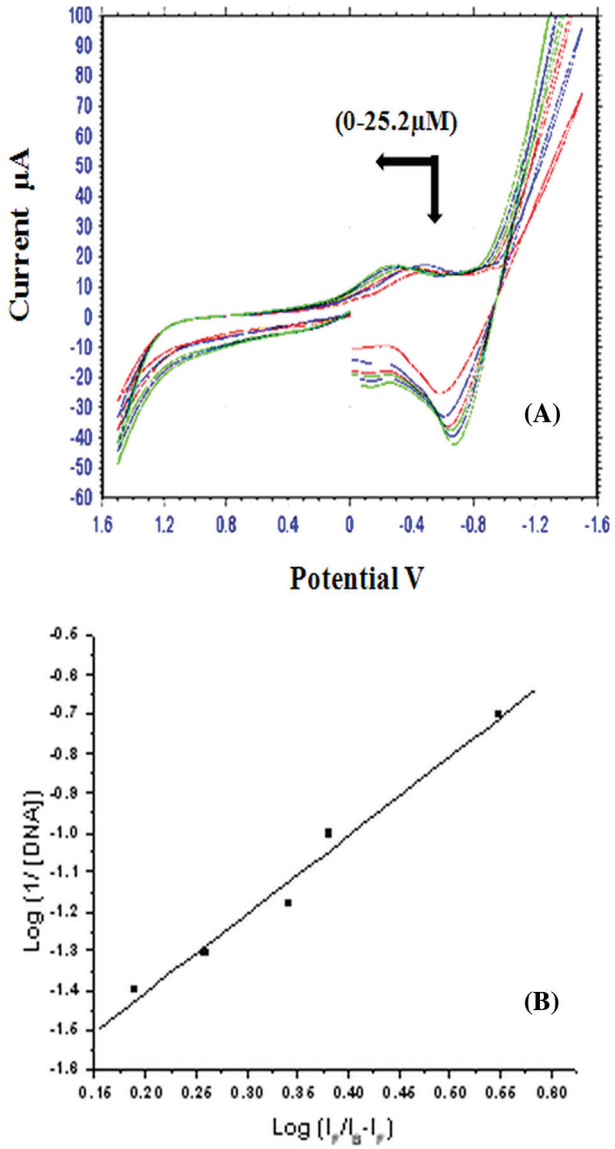

Fig. 13 (A) The voltammogram of CPNPs (12.07 µM) with stepwise addition of ST-DNA up to the saturating concentration (25.2 µM), in the potential range +1.6 V to −1.6 V. (B) Log(1/[DNA]) *vs.* $\log(I_F/I_B - I_F)$ plot for the CPNP–DNA interaction.

DNA, assuring that CPNPs did not interact with the DNA backbone region.

FTIR study. To understand which chemical groups of DNA were responsible for interacting with CPNPs, an FTIR study was carried out. The comparison of the FTIR spectra of CPNP-bound and -unbound DNA (Fig. 12) showed that the peak height within 1056.55 cm^{-1} to 1083.17 cm^{-1}, corresponding to the characteristic phosphate groups of free DNA, was lowered due to CPNP binding. Moreover, CPNP binding caused (i) abolition of the peaks at 1595.43 cm^{-1} (corresponding to N–H amide bond) and 2918.06 cm^{-1} (corresponding to C–H stretch) and (ii) appearance of four new peaks at two different positions *viz.*, 1712.70 cm^{-1} (characteristic of C═O bond), 1627.55 cm^{-1} (characteristic of C═O amide bond) and 899.30 cm^{-1} and 839.47 cm^{-1} (both for ═C–H out of plane bending). All these changes signified that the CPNPs caused some kind of local deformations in DNA double helical structure due to steric crowding.

Cyclic voltammetric study. The voltammograms of CPNPs with stepwise addition of DNA up to its saturating concentration, in the potential range +1.6 V to −1.6 V, is shown in Fig. 13A. The current–voltage profile of CPNPs alone exhibited irreversible reductive response at anode potential −0.58 V *vs.* Ag/AgCl. Cyclic voltammetric studies of the stabilizing agent sodium citrate and the precursors diammonium hydrogen phosphate and calcium nitrate, used to prepare CPNPs, were separately carried out (results not shown). The voltammograms of sodium acetate and diammonium hydrogen phosphate separately displayed reductive responses at −0.75 V and −0.6 V, respectively, similar to that of CPNPs, whereas that of calcium nitrate displayed no redox response. Therefore, the sodium citrate present in CPNPs seemed to be the actual redox active species. The peak currents at the anodic and cathodic regions in the voltammogram of CPNPs shifted gradually to higher and lower potentials, respectively, with the stepwise addition of DNA, implying that the interaction between CPNPs and DNA was electrostatic and groove-binding in nature.[52] Moreover, from such a voltammogram of CPNPs titrated with DNA, the binding constant (K_b) of the interaction between CPNPs and DNA was determined from the equation $\log(1/[DNA]) = \log K_b + \log(I_F/I_B - I_F)$, where I_F and I_B were currents in the absence and presence of the DNA, respectively.[53] The nature of the equation shows that the plot of log(1/[DNA]) *vs.* $\log(I_F/I_B - I_F)$ gives a straight line and the value of K_b can be determined from the antilog of the intercept of the graph on the *y*-axis. Fig. 13B shows the log(1/[DNA]) *vs.* $\log(I_F/I_B - I_F)$ plot for the CPNP–DNA interaction, from which their binding constant was determined to be 1.59×10^4 M^{-1} at 303 K. This value of the binding constant was somewhat less than the value obtained from the UV-vis spectrophotometric result (7.697×10^4 M^{-1} at 303 K, Table 1), however, the strength of interaction in both the cases was of the order of 10^4 M^{-1}.

AFM study. The DNA–CPNP interaction was visualized from the AFM image of their bound complex (Fig. 14). Fig. 14A shows the image of the ST-DNA population, where the average diameter of the DNA was measured to be about 1 µm in size. Since from the Watson–Crick structure the diameter of double helix was known to be 2 nm, each string-like DNA image of the population represented a bundle of approximately 500 individual DNA molecules. As a higher concentration of DNA (than that used in other studies) was required to visualize them by AFM, therefore, either or all of the factors such as (a) higher concentration of DNA, (b) presence of high positive charges for nickel cloud on mica surface, on which DNA sample was taken and (c) vacuum drying force to prepare the AFM sample, perhaps, was/were responsible for the aggregation of DNA molecules to bundles. Fig. 14B and C represent the close 2D and 3D views respectively of the bundle marked by the arrow in Fig. 14A. Fig. 14D shows the image of DNA incubated with CPNPs, where both DNA-bound and -unbound CPNPs were

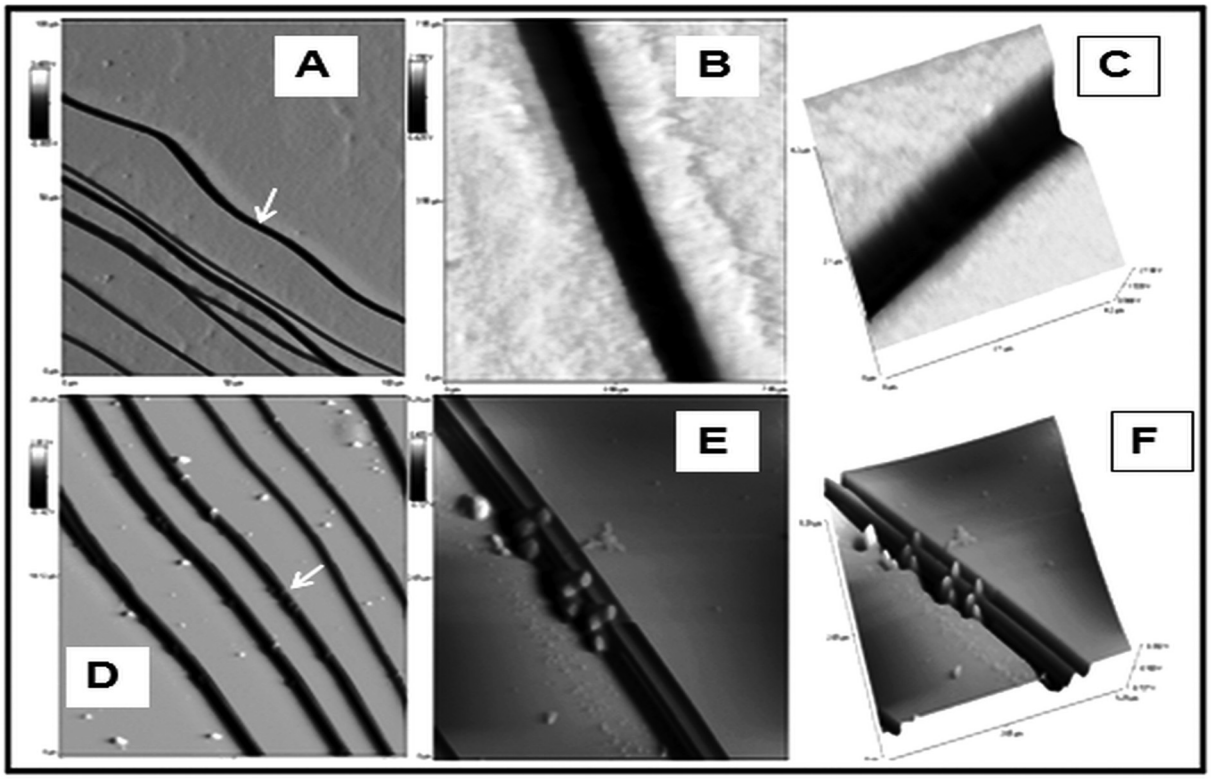

Fig. 14 AFM images of free and CPNP-bound ST-DNA. (A) Population of DNA bundles, (B) 2-D image of the DNA bundle marked by arrow in 'A', (C) 3-D image of the DNA bundle in 'A', (D) population of CPNP–DNA complex, (E) 2-D image of the region adjacent to the DNA marked by arrow in 'D', (F) 3-D image of the DNA in 'D'.

observed. Fig. 14E and F represent the close 2D and 3D views respectively of the DNA bundle marked by the arrow in Fig. 14D. The NPs appeared to be round in shape (as was observed in Fig. 3) and when their size was determined, the unbound free NPs were of average size 60 nm (as was determined from Fig. 3A), whereas those bound on DNA surface were of 200 nm in size. This apparent increase in size of the NP might be due to the close proximity of the NPs bound over different DNA molecules of a bundle.

Conclusion

In this communication first, we report a simple and fast method of synthesis of stable colloidal CPNPs, innovated by us.

Second, the prepared NPs were characterized for their average size, shape, zeta potential, molecular weight and composition. The NPs were nearly spherical in shape having a size, zeta potential and molecular weight of around 45 nm, −(23) mV and (250 ± 30) kDa, respectively; they were composed of the hydroxyapatite form of calcium phosphate and over 90% of the precursors were converted to the nano-form.

Third, the CPNP–DNA interaction was studied using various biophysical techniques. Our investigations revealed that (i) the DNA and CPNPs interacted at a stoichiometry of 3.26 : 1 and their binding interaction was cooperative, spontaneous, exothermic, enthalpy-driven and partially electrostatic in nature, (ii) the zone of interaction of DNA with CPNP was the groove region *i.e.*, the interaction occurred through groove binding mode, not through intercalation of the NPs within the base pairs of DNA; moreover, no alteration of the enzymatic and chemical digestion pattern of CPNP-bound DNA and free DNA made it evident that CPNPs did not interact with the phosphate backbone of DNA, (iii) a single nanoparticle interacted covering a stretch of 6 base pairs region of DNA, and (iv) the CPNP binding altered the native B-form of DNA to the less stacked and less helical C-form, albeit increasing the melting temperature of DNA by about 4 °C.

A question might be raised as to whether a particle of size 45 nm could bind to DNA grooves of size about 8 nm (minor groove) to 12 nm (major groove). In support, there have been reports[54–57] that ligands (nanoparticles/biopolymers) of sizes larger than that of the DNA grooves could act as groove-binding agents, where a minor part of the nanoparticle or biopolymer surface formed H-bonds/stacking bonds with DNA bases at the grooves, keeping the major part out of the grooves. In CPNPs, the stabilizing coat of Na-citrate perhaps formed H-bonds with DNA bases and contributed a part to the non-polyelectrolyte effect of the interaction. Presently, a work plan is in progress in our laboratory to unravel in molecular detail which chemical moieties and which different weak

interactions *viz.*, H-bonding, van der Waals interaction and hydrophobic interaction contributed to the dominant non-polyelectrolyte effect (about 72%) and which chemical moieties bound through weak electrostatic bonds contributed to the polyelectrolyte effect (about 28%) of the interaction between DNA and CPNPs.

Acknowledgements

We are indebted to the Department of Biotechnology, Government of India for financial assistance (project no. BT/PR11477/NNT/28/416/2008). We also acknowledge the Department of Science and Technology, Govt. of India for its 'FIST Programme – 2001–2011' & 'PURSE Programme – 2012–15', and the University Grants Commission, Govt. of India for its 'Special Assistance Program – 2011–16' going on in our department/university to provide the different instrumental and infrastructural support. We gratefully acknowledge Prof. S. Basak, Nuclear Chemistry Division, Saha Institute of Nuclear Physics, Dr Nilmoni Sarkar of the Department of Chemistry, IIT-Kharagpur, West Bengal, Dr Swarup Chattopadhhyay of Department of Chemistry, University of Kalyani, West Bengal and Dr Sukhen Das of Department of Physics, Jadavpur University, Kolkata for providing us the CD, viscometer, cyclic voltammeter and XRD facilities, respectively.

References

1 F. L. Graham and A. J. van der Eb, *Virology*, 1973, **52**, 456–467.
2 D. Lechardeur, A. S. Verkman and G. L. Lukacs, *Adv. Drug Delivery Rev.*, 2005, **57**, 755–767.
3 D. Oltona, J. Li, M. E. Wilsona, T. Rogers, J. Closed, L. Huange, P. N. Kumta and C. Sfeir, *Biomaterials*, 2007, **28**, 1267–1279.
4 E. V. Giger, J. Puigmartí-Luis, R. Schlatter, B. Castagner, P. S. Dittrich and C. Leroux, *J. Controlled Release*, 2011, **150**, 87–93.
5 Y. C. Liu, T. Wang, F. L. He, Q. Liu, D. X. Zhang, S. L. Xiang, S. P. Su and J. Zhang, *Int. J. Nanomed.*, 2011, **6**, 721–727.
6 V. Sokolovaa, H. R. Radtkeb and M. Epple, *Biomaterials*, 2006, **27**, 3147–3153.
7 V. Sokolova, A. Kovtun, O. Prymak, W. Meyer-Zaika, E. A. Kubareva, E. A. Romanova, T. S. Oretskaya, R. Heumannc and M. Epple, *J. Mater. Chem.*, 2007, **17**, 721–727.
8 R. Murugan and S. Ramakrishna, *Compos. Sci. Technol.*, 2005, **65**, 2385–2406.
9 C. G. Vazquez, C. P. Barba and N. Munguia, *Rev. Mex. Fis.*, 2005, **51**, 284–293.
10 M. P. Ferraz, F. J. Monteiro and C. M. Manuel, *J. Appl. Biomater. Biomech.*, 2004, **2**, 74–80.
11 M. Sadat-Shojai, *J. Iran. Chem. Soc.*, 2009, **6**, 386–392.
12 J. S. Earl, D. J. Wood and S. J. Milne, *J. Phys. Conf. Ser.*, 2006, **26**, 268–271.
13 K. Lin, J. Chang, R. Cheng and M. Ruan, *Mater. Lett.*, 2007, **61**, 1683–1687.
14 J. S. Cho and Y. C. Kang, *J. Alloys Compd.*, 2008, **464**, 282–287.
15 S. Bose and S. K. Saha, *Chem. Mater.*, 2003, **15**, 4464–4469.
16 G. K. Lim, J. Wang, S. C. Ng and L. M. Gan, *Langmuir*, 1999, **15**, 7472–7477.
17 M. Shirkhanzadeh and J. Mater, *Sci. Mater. Med.*, 1998, **9**, 67–72.
18 S. P. Mondéjar, A. Kovtun and M. Epple, *J. Mater. Chem.*, 2007, **17**, 4153–4159.
19 Q. He, A. R. Mitchell, S. L. Johnson, C. Wagner-Bartak, T. Morcol and S. J. D. Bell, *Clin. Vaccine Immunol.*, 2000, **7**, 899–903.
20 L. E. Alexander and H. P. Klug, *X-ray diffraction procedures for polycrystalline and amorphous material*, Wiley and Sons, New York, 1954, ch. 7, pp. 141–144.
21 S. G. Carter and D. W. J. Karl, *J. Biochem. Biophys. Methods*, 1982, **7**, 7–13.
22 B. D. N. Baron and J. L. Bell, *J. Clin. Pathol.*, 1959, **12**, 143–148.
23 K. E. van Holde, W. C. Johnson and P. S. Ho, *Principles of Physical Biochemistry*, Prentice-Hall, New Jersey, IMC, 2nd edn, 1998, ch. 15, pp. 614–615.
24 R. Persson, C. Wohlfart, U. Svensson and E. Everrit, *J. Virol.*, 1985, **54**, 92–97.
25 F. Barcelo, D. Capo and J. Portugal, *Nucleic Acids Res.*, 2002, **30**, 4567–4573.
26 C. E. Bostock-Smith and M. S. Searle, *Nucleic Acids Res.*, 1999, **27**, 1619–1624.
27 J. Sambrook and D. W. Russell, *Molecular Cloning*, Cold Spring Harbor Laboratory Press, New York, 3rd edn, 2001, ch. 5, vol. 1, pp. 5.4–5.13.
28 T. D. Tullius, *Free Radical. Res. Commun.*, 1991, **12–13**, 521–529.
29 J. Portugal and M. J. Waring, *FEBS Lett.*, 1987, **225**, 195–200.
30 Malvern – Zetasizer Nano – User manual, *Zeta potential theory*, England, man0317, 2008, ch. 16, pp. 1–12.
31 Malvern – Zetasizer Nano – User manual, *Molecular weight theory*, England, man0317, 2008, ch. 15, pp. 1–5.
32 F. Barrère, C. A. van Blitterswijk and K. de Groot, *Int. J. Nanomed.*, 2006, **1**(3), 317–332.
33 A. Milev, G. S. K. Kannangara and B. Ben-Nissan, *Mater. Lett.*, 2003, **57**, 1960–1965.
34 S. Bose and S. K. Saha, *Chem. Mater.*, 2003, **15**, 4464–4469.
35 L. Sun, L. C. Chow, S. A. Frukhtbeyn and J. E. Bonevich, *J. Res. Natl. Inst. Stand. Technol.*, 2010, **115**, 243–255.
36 C. Liao, F. Lin, K. Chen and J. Sun, *Biomaterials*, 1999, **20**, 1807–1813.
37 F. Barcelo, J. Martorell, F. Gavilaneq and J. M. Gonzalez-Rosz, *Biochem. Pharmacol.*, 1988, **37**(11), 2133–2138.
38 J. B. Chaires, *Annu. Rev. Biophys.. Biomol. Struct.*, 2008, **37**, 135–151.

39 C. E. Bostock-Smith and M. S. Searle, *Nucleic Acids Res.*, 1999, **27**(6), 1619–1624.
40 M. T. Record, C. F. Anderson and T. M. Lohman, *Rev. Biophys.*, 1978, **11**, 103–178.
41 J. B. Chaires, *Anticancer Drug Des.*, 1996, **11**, 569–580.
42 S. Das and G. S. Kumar, *J. Mol. Struct.*, 2008, **872**, 56–63.
43 R. R. Sinden, *DNA structure and function*, Academic Press, California, 1st edn, 1994, ch. 1, pp. 1–55.
44 S. Dongchul and J. B. Chaires, *Bioorg. Med. Chem.*, 1995, **3**(6), 723–728.
45 S. Tabassum, A. Asim, F. Arjmand, Md. Afzal and V. Bagchi, *Eur. J. Med. Chem.*, 2012, **58**, 308–316.
46 S. Roy, S. Saha, R. Majumdar, R. R. Dighe and A. R. Chakravarty, *Polyhedron*, 2010, **29**, 2787–2794.
47 B. Peng, X. Chen, K.-J. Dua, B.-L. Yua, H. Chao and L.-N. Ji, *Spectrochim. Acta, Part A*, 2009, **74**, 896–901.
48 U. Chaveerach, A. Meenongwa, Y. Trongpanich, C. Soikum and P. Chaveerach, *Polyhedron*, 2010, **29**, 731–738.
49 S. Panja, B. Jana, P. Aich and T. Basu, *Biopolymers*, 2008, **89**, 606–613.
50 J. D. McGhee, *Biopolymers*, 1976, **15**, 1345–1375.
51 D. M. Crothers, *Biopolymers*, 1971, **10**, 2147–2160.
52 N. Shahabadi and N. H. Moghadam, *Spectrochim. Acta, Part A*, 2012, **99**, 18–22.
53 N. Zhang, C. Xu, Q. Wei, B. Du, R. Li, T. Zhang, D. Wu and Y. Dai, *Adv. Mater. Lett.*, 2010, **1**(1), 34–39.
54 N. Prabakaran and P. Athappan, *J. Inorg. Biochem.*, 2010, **104**(7), 712–717.
55 K. Zhang, H. Fang, G. Shen, J. S. A. Taylor and K. L. Wooley, *Proc. Am. Thorac. Soc.*, 2009, **6**, 450–457.
56 W. Liua, S. Suna, Z. Caoa, X. Zhanga, K. Yaoa, W. W. Lub and K. D. K. Lukb, *Biomaterials*, 2005, **26**, 2705–2711.
57 C. Bailly, G. Chessari, C. Carrasco, A. Joubert, J. Mann, W. D. Wilson and S. Neidle, *Nucleic Acids Res.*, 2003, **31**, 1514–1524.